Length scales and self-organization in dense suspension flows

Gustavo Düring,[1,2] Edan Lerner,[1] and Matthieu Wyart[1]
[1]*Center for Soft Matter Research, Department of Physics, New York University, New York, New York 10002, USA*
[2]*Facultad de Física, Pontificia Universidad Católica de Chile, Casilla 306, Santiago, Chile*
(Received 9 October 2013; published 18 February 2014)

Dense non-Brownian suspension flows of hard particles display mystifying properties: As the jamming threshold is approached, the viscosity diverges, as well as a length scale that can be identified from velocity correlations. To unravel the microscopic mechanism governing dissipation and its connection to the observed correlation length, we develop an analogy between suspension flows and the rigidity transition occurring when floppy networks are pulled, a transition believed to be associated with the stress stiffening of certain gels. After deriving the critical properties near the rigidity transition, we show numerically that suspension flows lie close to it. We find that this proximity causes a decoupling between viscosity and the correlation length of velocities ξ, which scales as the length l_c characterizing the response to a local perturbation, previously predicted to follow $l_c \sim 1/\sqrt{z_c - z} \sim p^{0.18}$, where p is the dimensionless particle pressure, z is the coordination of the contact network made by the particles, and z_c is twice the spatial dimension. We confirm these predictions numerically and predict the existence of a larger length scale $l_r \sim \sqrt{p}$ with mild effects on velocity correlation and of a vanishing strain scale $\delta\gamma \sim 1/p$ that characterizes decorrelation in flow.

DOI: 10.1103/PhysRevE.89.022305 PACS number(s): 64.60.−i, 47.57.E−, 63.50.−x

I. INTRODUCTION

Although the emergence of rigidity is generally associated with the breaking of a continuous symmetry, amorphous materials acquire rigidity without such a symmetry change, by jamming in a random configuration. Non-Brownian suspensions of hard particles are a particularly interesting example of this phenomenon, where the control parameter is the anisotropy of the applied stress [1]. As the stress anisotropy is reduced and the solid phase is approached, the dynamics is reminiscent of critical phenomena. Correlated motion, or eddies, appear in the flow, whose characteristic length scale ξ seems to diverge [2]. Concomitantly, rheological properties are singular [1,3], as characterized most accurately in suspensions [4,5] where the viscosity η scales with the distance to jamming. Finally, a vanishing strain scale $\delta\gamma$ at which the structure reorganizes can be identified in experiments in which the direction of shear is reversed [6]. Understanding these properties at a microscopic level remains a challenge. A visually attractive image in sheared granular materials is that the dynamics is governed by the buckling of force chains, where stress is concentrated [7]. In another view dissipation is dominated by the formation of large eddies: Assuming that the latter act as regions where particles move as blocs, particle velocities are amplified as ξ increases, increasing dissipation and leading to a viscosity $\eta \sim \xi^2$ [8].

To quantify and discuss the validity of these views, we consider the affine solvent model (ASM) [8–13] where hard particles cannot overlap and where they receive a drag force proportional to their nonaffine velocity, i.e., their velocity with respect to an affinely moving fluid background. The ASM captures the existence of a diverging length scale [8,10,11], a vanishing strain scale [14], and displays singular rheological properties [10,12] similar to experiments [4]. In this model an analogy was derived between the rheological properties of hard particles and the elasticity of a network made of identical springs, corresponding to the contacts between particles [12]. Using this analogy, it was shown that if contact networks in flow were random, one would have $\eta \sim \xi^2 \sim 1/(z_c - z)$ [15], consistent with the idea that the length of eddies controls the viscosity. However, contact networks in flow are not random [12,16], but self-organize in configurations that are much harder to shear. The length scale l_c characterizing the response of the flow velocity to a local perturbation was predicted to be insensitive to this self-organization and to follow $l_c \sim 1/\sqrt{z_c - z}$ [15], while a simple assumption on the geometry of contact networks led to the prediction that $\eta \sim (z_c - z)^{-2.7}$, consistent with observations [16]. It is presently unclear if the length scale ξ describing velocity correlations is affected by this self-organization and is distinct from l_c and if the viscosity is tied to ξ. The relationship between self-organization and the vanishing strain scale at which configurations reorganize also remains not understood.

Here we shall argue that flow self-organizes into configurations where the buckling of force chains is very strong, leading to particle velocities and a divergence of the viscosity much larger than what is naively expected from the size of the eddies ξ, which we find to scale as l_c. A simple illustration of the buckling mechanism is a nearly straight chain of rigid rods immersed in a viscous fluid, compressed at its two ends, as shown in Fig. 1(e). As we shall see, under certain circumstances when the line is almost straight, the motion of the rods (and thus the dissipation) can be huge while velocity correlations are short ranged. We shall generalize the notion of buckling to floppy (undercoordinated) networks of rigid rods where the dynamics drive the system away from a configuration in which contact forces are balanced. Generically, floppy networks with $z < z_c$ are unstable and cannot balance contact forces. However, as anticipated by Maxwell [17] and discussed by Calladine [18], certain floppy configurations can satisfy force balance. A simple way to generate such configurations is to pull on a floppy network until it jams [see, for example, a sheared network of rigid rods in Fig. 1(a) and the simpler case of a linear chain under extensional flow in Fig. 1(d)]. It has been proposed [19–23] that this phenomenon generates the stress stiffening of biopolymer

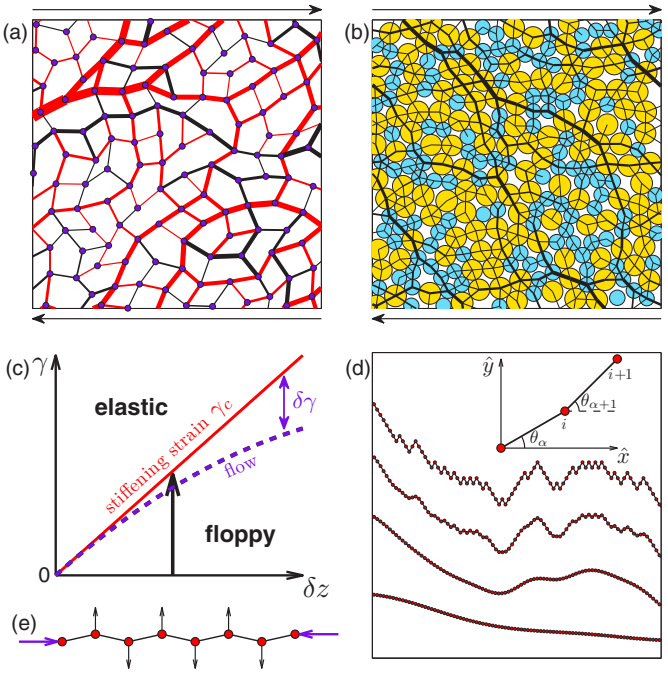

FIG. 1. (Color online) (a) Random floppy network under shear deformation approaching the SIJ transition; the thickness of the lines connecting the particles is proportional to the tension (red) or compression (black). Arrows indicate the direction of the shear. (b) Snapshot of a contact force network in the ASM of suspension flow, close to but below the jamming threshold. (c) Jamming phase diagram of networks in the coordination deficit $\delta z \equiv z_c - z$ and shear strain γ plane, showing the line of the shear-induced transition (red solid line) $\gamma_c \sim \delta z$ [20]. Our contention is that the contact networks in dense suspension flows lie very close to this stiffening line, thus defining a characteristic strain $\delta\gamma$ vanishing at jamming. (d) One-dimensional chain under an extensional flow at four different times. The vertical position of the chain has been shifted for clarity; the upper curve represents the initial configuration. (e) An almost straight chain buckling under compressive flow.

networks [24] responsible for the nonlinear response of certain biological tissues. This strain-induced jamming (SIJ) transition is the reverse process of what we will refer to here as the buckling transition. Apart from the case of certain crystals [25], these transitions are not well understood theoretically, even in simple models. In this paper we derive the scaling properties of the dynamics near these transitions, starting with the case of a line and extending our results to networks. A surprising result is that critical properties of SIJ depend on initial conditions, whereas its reverse process, the buckling transition, is universal. We then study the relationship between dense suspension flows and floppy networks pulled near jamming. We show numerically that configurations in suspension flows indeed lie very close to the buckling transition, as illustrated in Fig. 1(c), and use this result to make several predictions for dense flows.

II. ONE-DIMENSIONAL CHAIN

The case of a one-dimensional chain already illustrates the difference between the dynamics under pulling toward jamming (the SIJ transition) and pushing away from it (buckling). It also captures several critical dynamical properties that also apply to flow. We first consider the SIJ transition of a linear chain of N massless nodes (particles) connected by rigid rods of size a_0, immersed in a two-dimensional fluid of viscosity η_0, whose velocity profile corresponds to an extensional flow $\vec{\tilde{V}}_f = \dot{\gamma}(x\hat{x} - y\hat{y})$, where $\dot{\gamma}$ is the strain rate. This flow induces a drag force on the particles $\vec{\tilde{F}}_{drag} = \eta_0(\vec{\tilde{V}}_i - \vec{\tilde{V}}_f)$, where $\vec{\tilde{V}}_i$ corresponds to the velocity of particle i. If $\tilde{\tau}_\alpha$ is the tension in the rod α, balancing drag and contact forces read

$$\eta_0(\vec{\tilde{V}}_i - \vec{\tilde{V}}_f) = \tilde{\tau}_\alpha \vec{n}_{ii-1} + \tilde{\tau}_{\alpha+1}\vec{n}_{ii+1}, \tag{1}$$

where $\vec{n}_{ij}$ is the unit vector going from node i to j and α links the nodes $i-1$ and i. To obtain dimensionless expressions we define the strain $\gamma \equiv t\dot{\gamma}$, velocities $\vec{V} \equiv \vec{\tilde{V}}/\dot{\gamma}a_0$, and tensions $\tau \equiv \tilde{\tau}/\dot{\gamma}a_0\eta_0$. Introducing the angles θ_α made by the rod α and the horizontal x axis, as illustrated in the inset of Fig. 1(d), we can rewrite Eq. (1) by taking the difference of forces between two adjacent nodes and projecting it along the unit vector $\vec{n}_{ij}$ and along the unit vector perpendicular to $\vec{n}_{ij}$,

$$f_{ext} = \tau_{\alpha+1}\cos(\Delta\theta_{\alpha+1}) - 2\tau_\alpha + \tau_{\alpha-1}\cos(\Delta\theta_\alpha), \tag{2}$$

$$\dot{\theta}_\alpha + f^*_{ext} = \tau_{\alpha+1}\sin(\Delta\theta_{\alpha+1}) + \tau_{\alpha-1}\sin(\Delta\theta_\alpha), \tag{3}$$

where $\Delta\theta_\alpha \equiv \theta_\alpha - \theta_{\alpha-1}$, $f_{ext} \equiv \cos(2\theta_\alpha)$, and $f^*_{ext} \equiv \sin(2\theta_\alpha)$. Since the rods are rigid, the radial relative velocity $\dot{a}_0$ of the nodes vanishes in Eq. (3). The extensional flow stretches the chain until it undergoes a strain-induced jamming transition when $\theta_\alpha = 0$ for all α, i.e., it becomes a straight line. Appendix A shows that near the transition the relative fluctuations of tension are negligible. Equation (2) then implies

$$\tau \equiv \langle\tau\rangle = -\langle\Delta\theta^2\rangle^{-1}, \tag{4}$$

where $\langle\cdots\rangle \equiv \frac{1}{N}\sum_\alpha \cdots$. Using this result in Eq. (3) yields

$$\dot{\theta}_\alpha = (\theta_{\alpha+1} - 2\theta_\alpha + \theta_{\alpha-1})/\langle\Delta\theta^2\rangle. \tag{5}$$

Equation (5) is a diffusion equation with a time-dependent diffusion constant. It implies that as the transition is approached, short-wavelength fluctuations of the chain vanish first, as seen in Fig. 1(d). Thus a time-dependent length scale l_{corr} (measured in units of a_0) characterizes the shape and most of the dynamics occur on that length scale.

Equation (5) can be solved by introducing the Fourier decomposition $\theta_\alpha(t) = \frac{1}{N}\sum_{k=0}^{N-1}\theta_k(t)e^{(2\pi i/N)k\alpha}$, leading to a closed equation for $\langle\Delta\theta^2\rangle$,

$$\langle\Delta\theta^2\rangle = \frac{4}{N^2}\sum_k |\theta_k(0)|^2 \exp\left(-2\nu_k\int_0^\gamma \frac{d\tau}{\langle\Delta\theta^2\rangle}\right)\sin(\pi k/N)^2, \tag{6}$$

where $\nu_k = 2[1-\cos(\frac{2\pi k}{N})]$. Equation (6) depends on the initial angles $\theta_k(0)$. To illustrate this dependence, we consider random initial conditions whose Fourier components are independent and present a well-defined second moment $\overline{|\theta_k(0)|^2}/N = g(k)$, where the overbar denotes averaging over the distribution of initial conditions in the thermodynamic limit. We consider the family of initial conditions defined as $g(k) = \epsilon^2 c_\mu \sin(\pi k)^\mu$, with μ a non-negative even exponent

and c_μ a normalization constant such that $\int_0^1 g(k)dk = \epsilon^2$, where ϵ is the average amplitude of the initial angles. Further, $\mu = 0$ implies $g(k) = \epsilon^2$, meaning that the chain is initially a random walk. For $\mu \to \infty$, one gets $g(k) = \epsilon^2\delta(k - \frac{1}{2})$, which corresponds to a crystal with long-range order. For the given initial conditions, one can solve the asymptotic behavior of Eq. (6) in the thermodynamic limit to obtain

$$\langle \Delta\theta^2 \rangle \propto (\gamma_c - \gamma)^{(3+\mu)/(1+\mu)}, \tag{7}$$

$$\langle V^2 \rangle = \tau \propto (\gamma_c - \gamma)^{-(3+\mu)/(1+\mu)}, \tag{8}$$

$$\langle \dot{\theta}^2 \rangle \propto (\gamma_c - \gamma)^{-1}, \tag{9}$$

where $\gamma_c = \epsilon^2/2$. The equality in Eq. (8) stems from balancing the invested work per unit time per unit length $\eta_0 \sum_i \tilde{V}_i^2/a_0 N = \eta_0 \dot{\gamma}^2 a_0 \langle V^2 \rangle$ with the dissipation rate per unit length $\tilde{\tau}\dot{\gamma} = \eta_0 \dot{\gamma}^2 a_0 \tau$. The scaling of these quantities results from Eqs. (4) and (7). Equation (9) can be obtained from the simple geometrical consideration that the additional horizontal strain needed to reach the transition is $\gamma_c - \gamma = 1 - \langle \cos(\theta_\alpha) \rangle$. The results are that (i) initial conditions affect the critical properties and (ii) relative velocities, which are of the order of $\dot{\theta}$ [Eq. (9)], and absolute velocities V [Eq. (8)], do not scale in the same way in general, except for $\mu = \infty$. The prediction for the scaling of $\langle V^2 \rangle$ is tested in Fig. 2(b).

The diffusive dynamics imply that a length scale $l_{\rm corr}$ grows with strain. This length is picked up by velocity correlations, which can be obtained from Eqs. (5) and (7):

$$C(n) \equiv \langle \vec{V}_i \cdot \vec{V}_{i+n} \rangle \sim \left(\frac{n}{l_{\rm corr}} \right)^{2+\mu} e^{-(n/l_{\rm corr})^2}, \tag{10}$$

$$l_{\rm corr} \sim \left(\int_0^t \frac{d\tau}{\langle \Delta\theta^2 \rangle} \right)^{1/2} \sim (\gamma_c - \gamma)^{-1/(1+\mu)}, \tag{11}$$

in good agreement with the results of Fig. 2(e).

A second and larger length scale diverges near the transition and can be identified from the response to a local perturbation, defined as follows: At some time the driving flow is stopped and one single contact β is elongated at some rate, leading to a dipole of force of amplitude τ_0 on the two nodes adjacent to β. The response to such a local perturbation is described by Eq. (2), where the external force $f_{\rm ext}$ is now $f_\alpha = \delta_{\alpha,\beta}\tau_0$. Equation (2) can be written in matrix form using the bra-ket notation $\tau_0|\beta\rangle = -\mathcal{N}|\tau\rangle$, where $\langle\alpha|\tau\rangle = \tau_\alpha$, $\langle\alpha|\beta\rangle = \delta_{\alpha,\beta}$ and the $\mathcal{N}$ matrix is given by

$$\mathcal{N}_{\alpha\beta} = 2\delta_{\alpha,\beta} - \cos(\theta_\alpha - \theta_\beta)(\delta_{\beta,\alpha+1} + \delta_{\beta,\alpha-1}). \tag{12}$$

Inverting the $\mathcal{N}$ matrix is difficult in general. However, close to the critical point Appendix A shows that $\mathcal{N}$ can be approximated by its average value $\mathcal{N}_a \equiv \langle \mathcal{N} \rangle$. Translational invariance implies that the eigenvectors of $\mathcal{N}_a$ are plane-wave modes, with eigenvalues $\omega_q^2 = 2[1 - (1 - \langle \Delta\theta^2 \rangle/2)\cos(2\pi q/N)]$, where q is the wave number. The point response then reads

$$\tau_n = -\tau_0 \langle \beta + n|\mathcal{N}_a^{-1}|\beta\rangle \sim \tau_0 \sum_q e^{i2\pi qn}/\omega_q^2 \sim \tau_0 e^{-|n|/l_r},$$

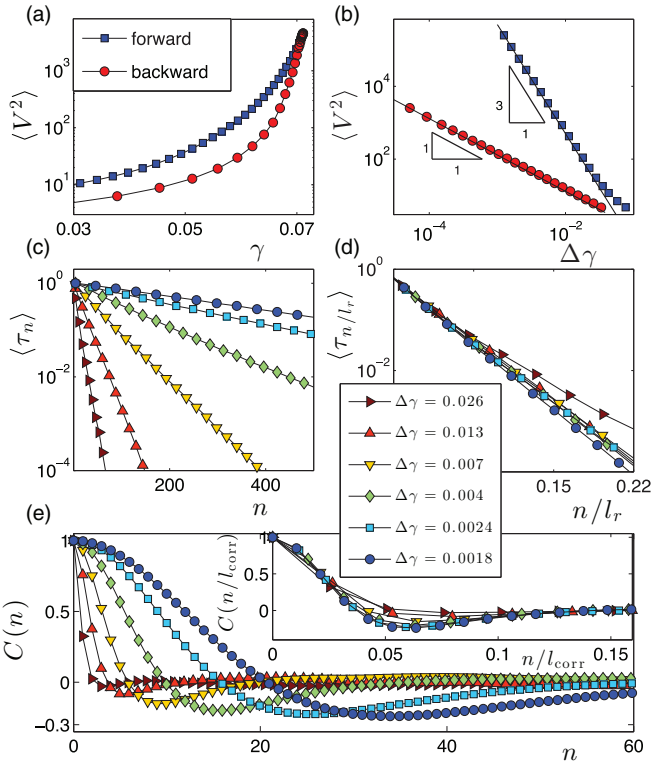

FIG. 2. (Color online) Properties of a one-dimensional chain stretched by an extensional flow with $N = 10\,000$ under periodic boundary conditions (see Appendix D for details on the numerical methods used). The initial distribution of the angles is random (i.e., $\mu = 0$). (a) $\langle V^2 \rangle = \tau$ versus strain γ. The blue squares describe the evolution toward the strain-induced jamming point and the red circles describe the buckling transition. The reversibility of the backward evolution breaks at some strain $\gamma_{\rm noise}$. The only source of noise is roundoff error. (b) A log-log plot of $\langle V^2 \rangle$ versus the distance to the critical point $\Delta\gamma$. The predicted exponent are 3 and 1, in perfect agreement with the simulations. (c) Average response to a local perturbation $\langle \tau_n \rangle$ vs the distance n to the perturbation. (d) Rescaled average response $\langle \tau_n \rangle$ vs rescaled distance $n/l_r \sim n\Delta\gamma^{3/2}$. (e) Average velocity correlation $C(n)$ vs the distance n. The inset shows the rescaled average velocity correlation $C(n)$ vs rescaled distance $n/l_{\rm corr} \sim n\Delta\gamma$.

where n is the distance to the perturbation and

$$l_r = 1/\sqrt{\langle \Delta\theta^2 \rangle} \sim (\gamma_c - \gamma)^{-(3+\mu)/(2+2\mu)} \tag{13}$$

is measured in units of a_0. Our third key result is thus that the SIJ transition in the linear chain is characterized by two length scales: $l_{\rm corr}$, which characterizes the velocity correlations, and l_r, which characterizes the response to a local perturbation. These length scales are tested numerically in Figs. 2(c)–2(e).

Buckling. The dynamics described by Eq. (5) are formally reversible. However, we find that if the strain rate is reversed at some strain γ_f smaller than but close to γ_c, the observed trajectory is not reversible, as shown in Figs. 2(a) and 2(b). Instead, in this backward evolution the dynamics become dominated by high spatial frequencies of the structure and are well described by Eqs. (7)–(9) and (13) with $\mu = \infty$ and some effective critical strain $\tilde{\gamma}_c < \gamma_c$, as shown in Appendix B. The correlation length follows $l_{\rm corr} \approx 1$. All these results are

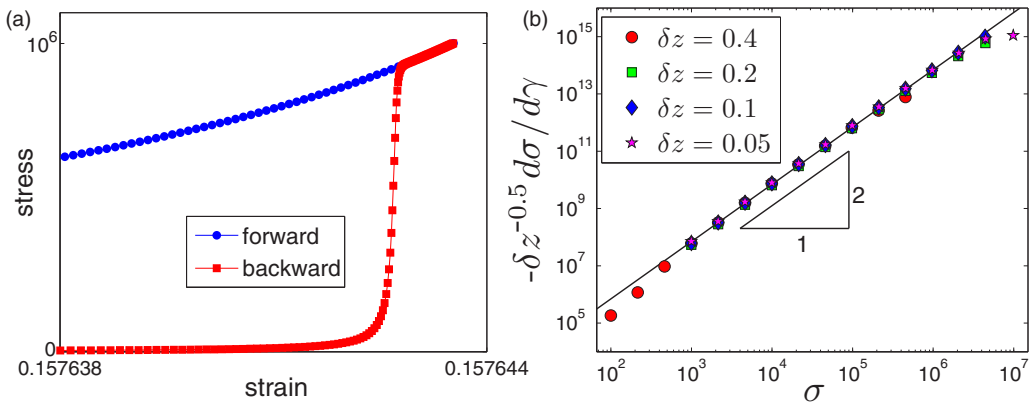

FIG. 3. (Color online) Two-dimensional network, built as in [20], under shear. (a) Stress σ vs strain γ. The blue circles represent the dynamics towards the SIJ transition, whereas the red squares represent the buckling transition. (b) Scaling of $\frac{d\sigma}{d\gamma}/\delta z^{0.5}$ vs σ in the vicinity of the buckling transition (see Appendix D for details about numerical methods). The slope of the line is the predicted exponent 2.

independent of the initial conditions: In contrast with the forward process, the reverse process is universal.

These results stem from the simple fact that when time is reversed, the tension in the rods changes sign (i.e., becomes compressive) and the diffusion coefficient of Eq. (5) becomes negative, which results in the amplification of high-frequency noise. Physically, this means that upon reversing the strain rate, the chain buckles on the smallest available length scale, leading to the universal results $\langle \Delta\theta^2 \rangle = \tilde{\gamma}_c - \gamma$, where $\tilde{\gamma}_c - \gamma_f \propto \langle \Delta\theta(\gamma_f)^2 \rangle$, as shown in Appendix B.

III. NETWORKS

Our results on the linear chain apply more generally to networks of N_c rigid rods connecting N nodes in spatial dimension d, immersed in a flowing solvent [see an example in Fig. 1(a)]. Unlike the case of the linear chain, in networks the coordination $z = 2N_c/N$ can be manipulated. Varying this parameter allows us to study the interplay between the rigidity transition that occurs in disordered isotropic networks when springs are added up to z_c, which is known to be associated with a diverging length scale $l_c \sim 1/\sqrt{\delta z}$ [15], and the SIJ transition. We consider floppy networks having $\delta z \equiv z_c - z > 0$; it has been shown that when deformation is imposed on such networks, they eventually undergo a SIJ transition at some strain $\gamma_c \sim \delta z$ [20]. At γ_c the velocities diverge, which implies a divergence of the stress and tension, as in the linear chain case. We focus on the buckling process. As in the case of the linear chain [compare Fig. 3(a) with Fig. 2(a)], a time-reversed diffusive process is the source of the irreversibility upon the backward dynamics. We thus expect this process to follow the same dependence on strain as the buckling of a linear chain, in particular that the dimensionless shear stress $\sigma \equiv \tilde{\sigma}/a_0\eta_0\dot{\gamma}$ (which plays the role of the dimensionless tension τ for the chain) follows $\sigma \sim C(\delta z)/(\gamma_c - \gamma)$ or, equivalently, $d\sigma/d\gamma \sim -\sigma^2/C(\delta z)$, where $C(\delta z)$ is some function whose derivation is left for future work. These predictions are tested numerically in random networks of rigid rods under simple shear with the driving flow $\vec{\tilde{V}}_f = \dot{\gamma} y \hat{x}$ (see Appendix D for numerical methods). Results are shown in Fig. 3(b), which supports that $C(\delta z) \sim 1/\delta z^{0.5}$.

A. Spectrum

In the buckling process, we expect that the structural length scale $l_{\rm corr}$ plays no role, as for the linear chain. We are thus left with two length scales at play: the length l_r associated with the SIJ transition and l_c associated with the rigidity transition. To disentangle the role of these, it is convenient to extend the definition of the linear operator $\mathcal{N}$ introduced for the chain in Eq. (12) to higher-dimensional networks. Following Calladine [18], we first introduce the operator $\mathcal{S}$ of dimension $N_c \times Nd$, with components $\mathcal{S}_{\alpha k} = (\delta_{j,k} - \delta_{i,k})\vec{n}_{ij}$, where α labels the rod connecting the node i with node j. It is easy to check that $\mathcal{S}^T|\tilde{\tau}\rangle \equiv |\tilde{F}_u\rangle$ is the set of unbalanced forces appearing on the nodes if the rod contact forces are $|\tilde{\tau}\rangle$, whereas $S|\tilde{V}\rangle$ is the rate at which rods change length if nodes were moving with a velocity $|\tilde{V}\rangle$ [18]. In our notation $\vec{\tilde{V}}_i = \langle i|\tilde{V}\rangle$. If a fluid with a velocity field $|\tilde{V}_f\rangle$ is creating a drag force $|\tilde{F}_{\rm drag}\rangle = \eta_0(|\tilde{V}_f\rangle - |\tilde{V}\rangle)$ on the nodes, it is easy to show (see [12] or Appendix C) that the contact forces $|\tilde{\tau}\rangle$ appearing on the rods follow

$$-\eta_0 \mathcal{S}|\tilde{V}_f\rangle = \mathcal{N}|\tilde{\tau}\rangle, \tag{14}$$

where $\mathcal{N} \equiv \mathcal{S}\mathcal{S}^T$ and $\mathcal{N}$ is symmetric and can be diagonalized $\mathcal{N} = \sum_\omega \omega^2 |\phi(\omega)\rangle\langle\phi(\omega)|$. Equation (14) shows that the contact forces, and hence the stress, can diverge only if there are modes approaching zero frequency in $\mathcal{N}$. The spectral density $D(\omega)$ in isotropic random floppy networks can be computed theoretically; it presents a gap at some frequency $\omega^* \sim \delta z$, above which it plateaus, as shown in Fig. 4, and the characteristic scale of the modes at ω^* is $l_c \sim 1/\sqrt{\delta z}$ [15].

As the anisotropy increases additional features must enter in the spectrum. At γ_c a set of self-balancing rod forces $|\phi_0\rangle$ appears, which constitutes a zero mode of $\mathcal{N}$. Additional modes denoted by $|\phi_{\omega(k)}\rangle$ must be present below ω^*, which correspond approximatively to plane-wave modulations of $|\phi_0\rangle$ [16]: $\langle\alpha|\phi_{\omega(k)}\rangle \approx \langle\alpha|\phi_0\rangle \exp(i2\pi\vec{r}_\alpha \cdot \vec{k})$, where $\vec{r}_\alpha$ is the position of contact α. Their frequency follows $\omega(k)^2 = \langle\phi_{\omega(k)}|\mathcal{N}|\phi_{\omega(k)}\rangle \approx Ak^2$, where A is a constant, leading to a Debye density of states below ω^* with $D(\omega) \sim \omega^{d-1}$. In our finite-size simulations only a few such modes can be visualized; an example is indicated by an arrow in Fig. 4(a).

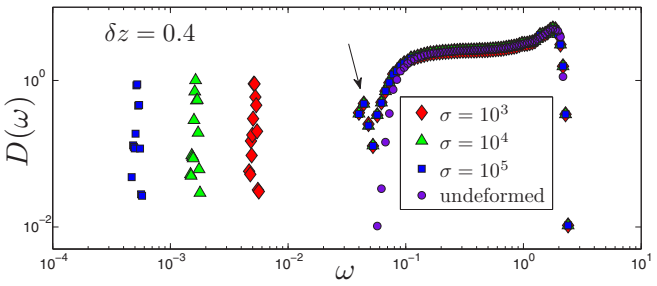

FIG. 4. (Color online) Spectral density $D(\omega)$ of the $\mathcal{N}$ operator for two-dimensional networks of size $N = 4096$, measured numerically for $\delta z = 0.4$ at various stresses, as indicated in the legend. In undeformed networks a gap is observed in $D(\omega)$ up to a frequency $\omega^* \sim \delta z$ [15]. Above ω^*, $D(\omega)$ remains effectively unchanged under the deformation, whereas below ω^* a single mode of frequency $\omega_{\min}$ rises from zero as $1/\sqrt{\sigma}$ (at constant z) upon buckling, for which $\sigma \to \infty$. Notice that $D(\omega)$ displays modes between $\omega_{\min}$ and ω^* indicated by the arrow; these are plane-wave modulations of the minimal mode and thus scale like $1/L$.

When buckling occurs as γ decreases below γ_c, contact forces are not balanced anymore and the minimal eigenvalue $\omega^2_{\min}$ of $\mathcal{N}$ rises from zero as shown in Fig. 4. Near γ_c the stress will be governed by this minimal mode $|\phi_0\rangle$, as can be deduced from a spectral decomposition of Eq. (14), implying that the norm of the dimensionless contact forces $\tau \equiv \tilde{\tau}/a_0\eta_0\dot{\gamma}$ follows $||\tau|| \sim 1/\omega^2_{\min}$ (with some coordination-dependent prefactor). Since shear stress and contact forces are proportional, we obtain $\omega_{\min} \sim C_2(\delta z)/\sqrt{\sigma}$, where $C_2(\delta z)$ is some function. We find numerically and will justify elsewhere that for isotropic networks that are pulled near the SIJ transition, $C_2(\delta z) \sim \sqrt{\delta z}$. As for the zero mode at γ_c, there are also modes in the spectrum of $\mathcal{N}$ corresponding to plane-wave modulation of the minimal mode, easily shown to lead to a density of states $D(\omega) \sim \omega(\omega^2 - \omega^2_{\min})^{(d-2)/2}$ for $\omega < \omega^*$.

B. Length scales

We can now consider the point response of networks, obtained by changing the length of a single rod β at a rate of t_0^{-1} at a fixed strain γ. This procedure corresponds to replacing $S|\tilde{V}_f\rangle$ by $t_0^{-1}|\beta\rangle$ in Eq. (14), giving rise to the rod forces $|\tilde{\tau}\rangle = \eta_0 t_0^{-1}\mathcal{N}^{-1}|\beta\rangle$. Consequently, the dimensionless force $\tau_\alpha \equiv \tilde{\tau}_\alpha t_0/\eta_0$ in a rod α due to elongating the rod β is given by $\langle\alpha|\tau\rangle = \langle\alpha|\mathcal{N}^{-1}|\beta\rangle$. Using an eigenvalue decomposition of the $\mathcal{N}$ operator, we identify and collect separately the contributions to $\langle\alpha|\tau\rangle$ stemming from modes having frequencies $\omega > \omega^*$ and $\omega < \omega^*$, denoted in the following by $\langle\alpha|\tau\rangle_*$ and $\langle\alpha|\tau\rangle_{\min}$. The modes above ω^* are statistically equivalent to those of undeformed random networks, for which it is known that $\langle\alpha|\tau\rangle_* \sim e^{-r/l_c}$ [15] with an additional algebraic prefactor of r that depends on the spatial dimension, where $r \equiv |\vec{r}_\alpha - \vec{r}_\beta|$ and $l_c \sim \delta z^{-1/2}$.

The contribution stemming from the modes below ω^* can be calculated using the modes $|\phi_{\omega(k)}\rangle$ introduced above, leading to

$$\langle\alpha|\tau\rangle_{\min} = \sum_{\omega(k)<\omega*} \frac{\langle\phi_0|\beta\rangle\langle\alpha|\phi_0\rangle \exp[i2\pi(\vec{r}_\alpha - \vec{r}_\beta)\cdot\vec{k}]}{\omega^2_{\min} + A\,k^2}.$$

The sum over these plane-wave modes is dominated by the low wave numbers k. Taking the continuum limit, we obtain an exponential decay in the response for large r:

$$\langle\alpha|\tau\rangle_{\min} \sim \langle\phi_0|\beta\rangle\langle\alpha|\phi_0\rangle e^{-r/l_r}, \tag{15}$$

where $l_r \sim 1/\omega_{\min}$. The factor $\langle\alpha|\phi_0\rangle$ can fluctuate from rod to rod, but since $|\phi_0\rangle$ is an extended mode it does not decay with the distance r.

Both contributions $\langle\alpha|\tau\rangle_{\min}$ and $\langle\alpha|\tau\rangle_*$ have exponential decays, but on different length scales l_r and l_c. To determine which is the dominant length scale, we need to estimate the relative amplitude of each contribution. This can be done by calculating the total norm of the rod forces $||\tau||^2$, which reads

$$\langle\tau|\tau\rangle = \langle\beta|\mathcal{N}^{-2}|\beta\rangle = \underbrace{\sum_{\omega^*>\omega} \frac{\langle\phi(\omega)|\beta\rangle^2}{\omega^4}}_{\tau^2_{\min}} + \underbrace{\sum_{\omega^*<\omega} \frac{\langle\phi(\omega)|\beta\rangle^2}{\omega^4}}_{\tau^2_*}. \tag{16}$$

Using $\sum_\beta \langle\phi(\omega)|\beta\rangle^2 = 1$, one can express the average of these norms in the thermodynamic limit in terms of $D(\omega)$, leading to $\langle\tau^2_*\rangle \sim 1/\delta z^3$ and $\langle\tau^2_{\min}\rangle \sim \omega^{d-4}_{\min}$. We conclude that if $\delta z < \omega^{(4-d)/3}_{\min}$, the response to a local perturbation has an initial exponential decay on the scale l_c, which then crosses over to a much slower decay on the scale l_r for larger distances. However, close enough to the buckling transition, i.e., if $\omega^{(4-d)/3}_{\min} < \delta z$, the response in force is entirely controlled by l_r.

The dimensionless velocity field $|V\rangle = \frac{t_0}{a_0}|\tilde{V}\rangle$ in response to the same perturbation can also be calculated. This response must also have two terms decaying exponentially with length scales l_r and l_c, but the relative amplitudes of these terms turns out to differ from that of the force response. To determine the amplitude of each contribution, we estimate, as for the force response (16), their respective roles in the total norm of the velocity field $\langle V|V\rangle = \langle\beta|\mathcal{N}^{-1}|\beta\rangle = V^2_{\min} + V^2_*$. We find $\langle V^2_*\rangle \sim 1/\delta z$ and $\langle V^2_{\min}\rangle \sim \ln(\omega^*/\omega_{\min})$ in $d = 2$, or $\langle V^2_{\min}\rangle \sim \delta z^{d-2}$ in larger dimension. Thus, in terms of velocities for $d > 2$, the dominant response always decays as l_c and l_r can only be observed far from the deformed contact. Both the length scale and the amplitude of the response are in excellent agreement with the numerics (see Fig. 5) that reflect both the presence of strain-independent length l_c and a diverging length l_r.

Velocity correlations near the buckling transition are associated with the properties of the minimal mode $|\phi_0\rangle$, which are analytically hard to access. However, large networks can be simulated, allowing us to measure correlations adequately. We find that the correlations of velocities under shear are very similar to the velocity response to a point perturbation, as shown in Appendix E: They present an initial decay on the length l_c, followed by a decay of much milder amplitude on the length l_r, which is visible only for $r > l_c$. Thus networks near buckling present a clear decoupling between the dimensionless stress (diverging near buckling) and velocity correlations, mainly governed by l_c, which is independent of the distance to the buckling transition.

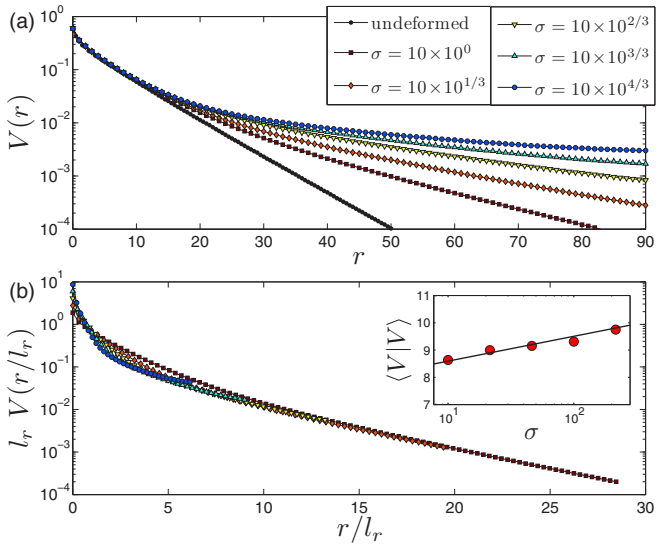

FIG. 5. (Color online) (a) Velocity field amplitude $V(r)$ as a response to a local perturbation vs the distance to the perturbation r for different shear stress in two dimensions. (b) Considering the predicted length scale $l_r \sim \sqrt{\sigma}$, the rescaled velocity $V(r/l_r)l_r$ vs rescaled distance r/l_r collapse on a single curve for a fixed coordination in agreement with the theory. The inset shows the total velocity field displacement $\langle V|V\rangle$ vs the stress σ, showing the predicted logarithmic increase.

IV. SUSPENSION FLOWS

In the ASM of suspension flows [8–13] contacts made between particles define a network, as shown in Fig. 1(b). The topology of the network evolves as contacts break and are formed during collisions [12]. At fixed volume and constant $\dot{\gamma}$, at discrete instants of time, contacts are formed, leading to abrupt jumps in the stress (infinitesimal as $N \to \infty$), which relaxes between collisions, as shown in Fig. 6(a). We make the hypothesis that the smooth motion in between collisions is dominated by the proximity of a buckling transition, leading to a decoupling between viscosity and the velocity correlation length. According to this hypothesis, our results on constructed networks near their buckling transition must apply to flow: No structural length $l_{\rm corr}$ should play a role, but the two lengths l_c and $l_r \sim 1/\omega_{\rm min}$ should enter in velocity correlations, whereas $\sigma \sim C'(\delta z)/(\gamma - \gamma_c)$ and $\omega_{\rm min} \sim C_2'(\delta z)/\sqrt{\sigma}$. The functions $C'(\delta z)$ and $C_2'(\delta z)$ can in principle differ from $C(\delta z)$ and $C_2(\delta z)$ introduced for networks because aspects of the respective networks are different: In flow (i) contact forces must be positive and (ii) near jamming the contact network has a nonvanishing anisotropy, i.e., the shear component of the stress does not vanish and $\sigma \sim p$ [12]. Both facts are in contrast to our constructed networks, for which forces can be negative and for which the anisotropy vanishes even at γ_c as $\delta z \to 0$ [20]. From these considerations, together with the additional hypothesis that nonaffine displacements and relative displacements between particles in contact are of the same order, it is straightforward to show (see Appendix C) that $C'(\delta z) \sim \delta z^0$ and $C_2'(\delta z) \sim \delta z^0$. These results imply that $d\sigma/d\gamma \sim -\sigma^2$, as confirmed numerically in Fig. 7(b) (see Appendix D for details about numerical methods). These predictions can also be tested by replacing contacts between particles in flow at some instant of time by rigid rods and by shearing the resulting network *backward*, until a SIJ transition occurs. We predict a transition for a backward strain of amplitude $\delta\gamma \equiv \gamma - \gamma_c \sim 1/\sigma$, as illustrated in Fig. 6(b). This result is checked in Fig. 7(a). Since observations in flow indicate $\sigma \sim \delta z^{-2.7}$ [12], we get $\delta\gamma \sim \delta z^{2.7} \ll \delta z$. These results support the hypothesis that suspension flows lie much closer to a buckling transition than isotropic random networks for which $\delta\gamma \sim \delta z$. It also yields a characteristic strain scale $\delta\gamma \sim 1/\sigma \sim 1/p$, in agreement with the numerical observation that particle velocities decorrelate on that strain scale [14].

Our scenario imposes that the spectrum of $\mathcal{N}$ presents a minimal mode at a frequency $\omega_{\rm min} \sim 1/\sqrt{\sigma}$, as previously

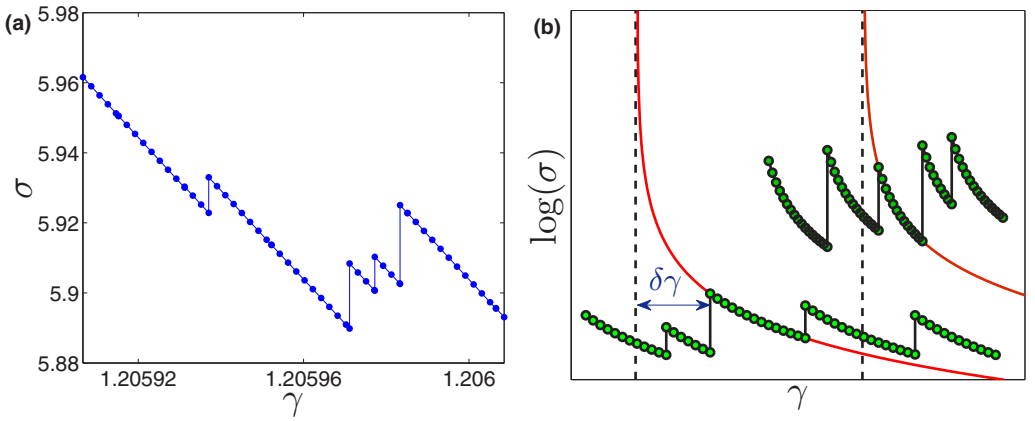

FIG. 6. (Color online) (a) Typical stress vs strain signal from the ASM simulations [12,26]. The stress relaxes between the abrupt increases that signal collisions of the sheared hard particles. The slope of the stress during the relaxation segments depends on the stress itself as $d\sigma/d\gamma \sim -\sigma^2$, as derived in Appendix C and validated numerically in Fig. 7(b). (b) Illustration of the relation between the stress relaxation in between collisions in the ASM and the buckling transition: The stress follows $\sigma \sim (\gamma - \gamma_c)^{-1}$ (red solid curves) between collisions, which is analogous to the stress relaxation of floppy networks evolving *away* from a buckling transition. The dashed vertical lines indicate the strain γ_c at which a floppy network, constructed by connecting the centers of the hard particles in contact by rods, would undergo a SIJ transition if it were sheared backward. We note that while the strain intervals between collisions (the length of the dotted curves) vanish in the thermodynamic limit, the strain scale $\delta\gamma \equiv \gamma - \gamma_c \sim 1/\sigma$ is independent of system size.

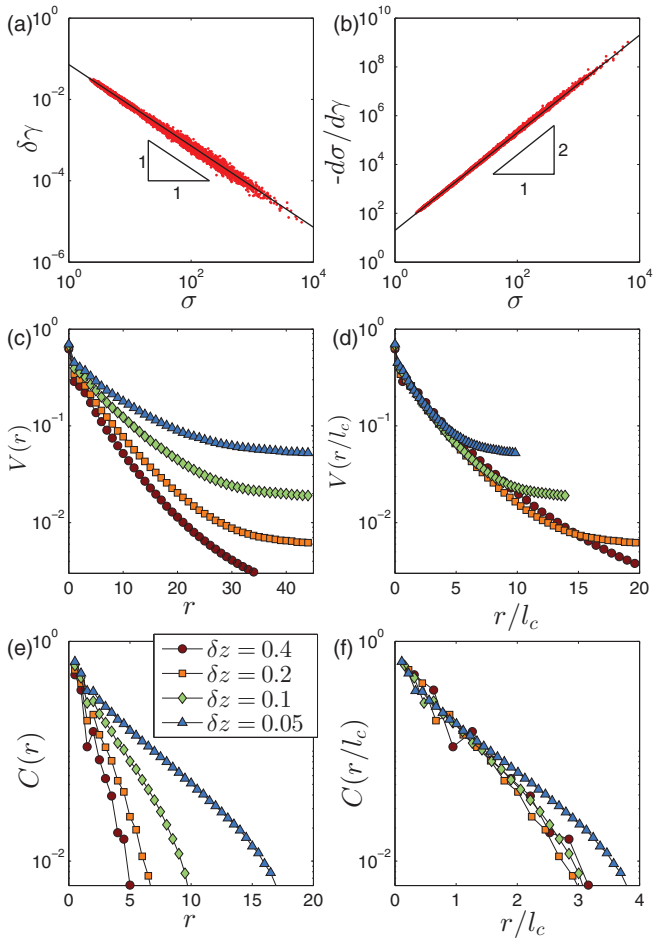

FIG. 7. (Color online) Hard-particle suspensions modeled by the ASM simulated as in [12]. (a) Distance in strain $\delta\gamma$ to the SIJ point (as explained in the text) vs the stress σ. (b) Scaling of $-\frac{d\sigma}{d\gamma}$ vs σ for hard-particle systems under shear flow. (c) Average velocity response to a local perturbation $V(r)$ vs the distance r to the perturbation. (d) Average response $V(r)$ vs the rescaled distance r/l_c. (e) Velocity correlation $C(r) \equiv \langle \vec{V}_i \cdot \vec{V}_j \rangle / \langle V^2 \rangle$ vs the distance r between particles i and j. (f) Velocity correlations $C(r)$ vs the rescaled distance r/l_c.

observed [12] and argued for [16]. Thus, following our results of the previous section on networks, we expect both the response to a local perturbation and the velocity correlations to be characterized by two length scales: $l_c \sim 1/\sqrt{\delta z}$ and a much larger $l_r \sim \sqrt{\sigma} \sim \sqrt{p}$, that should govern correlations only for $r \gg l_c$. Figure 7 confirms our central result that both the response to a point perturbation and velocity correlations decay as e^{-r/l_c}, as expected for $r \lesssim l_c$. For $r \gg l_c$ however, the characteristic decay length should be l_r, but this prediction is hard to test numerically as our system sizes are limited.

V. CONCLUSION

We have shown that the strain-induced jamming transition is akin to a critical point, but of a curious kind: When this transition is approached, exponents depend on the initial conditions and two length scales diverge. When going away from this transition, the associated buckling behavior becomes universal and only one singular length scale plays a role. Some of these results could help distinguish which processes control the nonlinear behavior of floppy gels. On the one hand, although our models are much simpler than gels of biopolymers, we expect our prediction that the nonaffine displacements of the network nodes spike when stiffening occurs to be robust; in fact, this was observed numerically in models that include bending elasticity [19] and has been recently related to the SIJ transition [21]. This prediction could be used to test when this scenario is responsible for the observed shear stiffening of these materials or when nonlinearities of the individual fibers are instead responsible, as initially proposed [27]. On the other hand, the presence of weak interactions (e.g., bending) was shown to affect qualitatively some aspects of the elastic response in floppy materials [15] and should be included in the future to obtain a description of the SIJ transition that applies quantitatively to gels.

Most importantly, we have argued that this same transition plays a role in simple models of suspensions flows (where weak interactions are absent), thus building a bridge between two quite distinct classes of materials. This approach has allowed us to characterize quantitatively the buckling of force chains and to propose a different perspective on the self-organization characterizing these driven materials. Our approach predicts a rather subtle scenario with a vanishing strain scale and two diverging length scales, whose dominant one diverges weakly as $l_c \sim 1/\sqrt{\delta z} \approx p^{-0.18}$ and is decoupled from the divergence of the viscosity. Our numerical observations strongly support this prediction. Our exponent for the divergence of l_c is smaller than early numerical estimates [8,10]. However, these numerics were performed in relatively small systems and the length was measured as a function of ϕ instead of p, which considerably increases finite-size effects. Although the presence of hydrodynamic interactions complicates the extraction of length scales from velocity correlations [28], measurements of the response to local perturbations, as well as studies of the nonlocal rheology [29,30], should enable us to test our predictions experimentally.

ACKNOWLEDGMENTS

We thank Eric DeGiuli for constructive comments on the manuscript. This work was supported by the Sloan Fellowship, National Science Foundation Grant No. DMR-1105387, Petroleum Research Fund Grant No. 52031-DNI9, and the MRSEC Program of the National Science Foundation Grant No. DMR-0820341. G.D. acknowledges partial support from CONICYT PAI/Apoyo al Retorno Grant No. 82130057.

APPENDIX A: PERTURBATION EXPANSION

In order to find an expression for the evolution we need to solve the force balance equation (2), which can be written as

$$\mathcal{N}|\tau\rangle = -|v_f\rangle, \tag{A1}$$

where $\langle\alpha|v_f\rangle = f_{\text{ext}} \equiv \cos(2\theta_\alpha)$ and the $\mathcal{N}$ matrix is defined in Eq. (12). In the linear chain the critical point corresponds to

a line (i.e., $\theta_\alpha = 0$ for all α), signaling that the natural small parameter should be small angles. A standard perturbation analysis around the critical point cannot be carried out because it is singular. Therefore, we introduce the parameter κ and write the $\mathcal{N}$ matrix as $\mathcal{N} = \mathcal{N}_\kappa + \delta\mathcal{N}_\kappa$, where

$$\langle\alpha|\mathcal{N}_\kappa|\beta\rangle = 2\delta_{\alpha,\beta} - (1-\kappa)\delta_{\beta,\alpha+1} - (1-\kappa)\delta_{\beta,\alpha-1}, \quad \text{(A2)}$$

$$\langle\alpha|\delta\mathcal{N}_\kappa|\beta\rangle = \left[\tfrac{1}{2}(\theta_\alpha - \theta_\beta)^2 - \kappa\right](\delta_{\beta,\alpha+1} + \delta_{\beta,\alpha-1}), \quad \text{(A3)}$$

and κ will be chosen to remove the singularity. Equation (A1) then reads $\mathcal{N}_\kappa|\tau\rangle = -|v_f\rangle - \delta\mathcal{N}_\kappa|\tau\rangle$, for which a solution can be formally written as a series

$$|\tau\rangle = -\mathcal{N}_\kappa^{-1}|v_f\rangle + \mathcal{N}_\kappa^{-1}\delta\mathcal{N}_\kappa\mathcal{N}_\kappa^{-1}|v_f\rangle - \mathcal{N}_\kappa^{-1}\delta\mathcal{N}_\kappa\mathcal{N}_\kappa^{-1}\delta\mathcal{N}_\kappa\mathcal{N}_\kappa^{-1}|v_f\rangle + \cdots. \quad \text{(A4)}$$

To calculate the contribution of the higher-order terms in the expansion (A4) we use the eigenvectors and eigenvalues of $\mathcal{N}_\kappa$, which are given by

$$\langle\alpha|\psi_q\rangle = \frac{e^{i2\pi q\alpha/N}}{\sqrt{N}}, \quad \omega_q^2 = 2[1-(1-\kappa)\cos(2\pi q/N)],$$

respectively. Here q is an integer in the interval $[0, N-1]$ and the contraction

$$\langle\psi_q|\delta\mathcal{N}_\kappa|\psi_l\rangle = (e^{2\pi il/N} + e^{-2\pi iq/N})\left(\frac{1}{2N}\Delta_{l-q} - \kappa\delta_{q,l}\right),$$

where $\Delta_q = \sum_{\alpha=0}^{N-1}(\theta_\alpha - \theta_{\alpha+1})^2 e^{2\pi iq\alpha/N}$ is the Fourier transform of $(\theta_\alpha - \theta_{\alpha+1})^2$. In the thermodynamic limit $|\Delta_q|^2/N$ is singular at $q = 0$ due to the nonzero mean of the real-space function. This singularity is precisely what we need to remove by taking

$$\kappa = \Delta_{q=0} = \frac{1}{2N}\sum_{\alpha=0}^{N-1}(\theta_\alpha - \theta_{\alpha+1})^2 = \langle\Delta\theta^2\rangle/2.$$

The minimal frequency $\omega_0^2 = 2\kappa$ is given by the mean square of the angle differences between neighboring nodes. Then $\mathcal{N}_\kappa$ corresponds precisely to the average $\langle\mathcal{N}\rangle$, where the spatial average is taken over the coefficients of the $\mathcal{N}$ matrix.

Close to the critical point θ_α can be considered small and $|v_f\rangle \approx \sqrt{N}|\psi_0\rangle$; therefore, the first term in the series (A4) leads to a constant tension $\tau_\alpha = -1/\langle\Delta\theta^2\rangle$, which corresponds to the average tension $\langle\tau\rangle$. In order to get an asymptotic expansion, the square of the average tension $\langle\tau\rangle^2 \equiv \langle v_f|\mathcal{N}_\kappa^{-2}|v_f\rangle$ must be larger than the amplitude of the fluctuations. From the expansion (A4) the amplitude of the first correction to the average is given by

$$\delta\tau^2 = \langle v_f|\mathcal{N}_\kappa^{-1}\delta\mathcal{N}_\kappa\mathcal{N}_\kappa^{-2}\delta\mathcal{N}_\kappa\mathcal{N}_\kappa^{-1}|v_f\rangle. \quad \text{(A5)}$$

The approximation is valid only if the ratio of the fluctuations' amplitude over the average amplitude satisfies

$$\frac{\delta\tau^2}{\langle\tau\rangle^2} = \sum_{q\neq 0}\frac{|\langle\psi_q|\delta\mathcal{N}_\kappa|\psi_0\rangle|^2}{\omega_q^4} \ll 1. \quad \text{(A6)}$$

A straightforward calculation leads to the expression for the overlap

$$|\langle\psi_q|\delta\mathcal{N}_\kappa|\psi_0\rangle|^2 = \frac{16}{N^3}\cos\left(\pi\frac{q}{N}\right)^2\sum_{k_1k_2}\theta_{k_2-q}\theta_{-k_2}\theta_{k_1+q}\theta_{k_1} \times \sin\left(\pi\frac{k_2-q}{N}\right)\sin\left(\pi\frac{k_2}{N}\right) \times \sin\left(\pi\frac{k_1+q}{N}\right)\sin\left(\pi\frac{k_1}{N}\right).$$

The final result depends on the distribution of the initial conditions for the angles $\theta_k(0)$. Considering distributions with small or no higher-order cumulant, the distribution can be taken as Gaussian. In this case the thermodynamic limit of the ratio $\frac{\delta\tau^2}{\langle\tau\rangle^2}$ is given by

$$\frac{\delta\tau^2}{\langle\tau\rangle^2} \approx 32c_\mu^2\int_0^1\frac{dkdq}{\omega_q^4}\cos(\pi q)^2\{\sin[\pi(k-q)]\sin(\pi k)\}^{\mu+2} \times \exp\left(-2(\nu_k+\nu_{k-q})\int_0^\gamma\frac{d\tau}{\langle\Delta\theta^2\rangle}\right), \quad \text{(A7)}$$

where we used $q/N \to q$ with $q \in [0,1]$. Equation (A7) results from the diffusion equation (5) and the statistical space homogeneity of the system. Notice that for the case of an initial distribution given by random independent angles $\theta_\alpha(0)$, expression (A7) is exact since it is Gaussian distributed. Finally, an upper bound can be obtained for Eq. (A7), taking $q = 0$, except at the denominator ω_q^4, which reads

$$\frac{\delta\tau^2}{\langle\tau\rangle^2} \lesssim \langle\Delta\theta^2\rangle^{(1+\mu/)(6+2\mu)} \sim (\gamma_c - \gamma)^{1/2}.$$

Thus, close to the critical point the approximation is valid and fluctuations can be neglected to a first approximation. An asymptotic behavior is expected for the higher-order contributions in the expansion (A4), but a detailed consideration is beyond the scope of the present paper.

APPENDIX B: EFFECT OF NOISE AND LOSS OF REVERSIBILITY

We shall consider the diffusion equation with a δ-correlated Gaussian noise

$$\dot\theta_\alpha = \frac{\dot\gamma}{\langle\Delta\theta^2\rangle}(\theta_{\alpha+1} - 2\theta_\alpha + \theta_{\alpha-1}) + \xi_\alpha(t), \quad \text{(B1)}$$

where $\langle\xi_\alpha(t)\xi_\beta(t')\rangle = \varsigma^2\delta_{\alpha,\beta}\delta(t-t')$. Notice that in this appendix, for sake of simplicity, we will not use a dimensionless time. Taking the Fourier transform, we obtain

$$\theta_k(t) = \theta_k(t_0)\exp\left(\dot\gamma\nu_k\int_{t_0}^t\frac{d\tau}{\langle\Delta\theta^2\rangle}\right) + \int_{t_0}^t\exp\left(\dot\gamma\nu_k\int_u^t\frac{d\tau}{\langle\Delta\theta^2\rangle}\right)\xi_k du, \quad \text{(B2)}$$

with the Fourier components $\xi_k = \sum_{\alpha=0}^{N-1} \xi_\alpha e^{-i2\pi k\alpha/N}$. The self-consistent equation (6) is now given by

$$\langle \Delta\theta^2 \rangle = \frac{4}{N} \sum_k g(k) \exp\left(2\dot\gamma \nu_k \int_{t_0}^{t} \frac{d\tau}{\langle \Delta\theta^2 \rangle} \right) \sin(\pi k/N)^2 + \varsigma^2 \frac{4}{N} \sum_k \int_{t_0}^{t} \exp\left(2\dot\gamma \nu_k \int_{u}^{t} \frac{d\tau}{\langle \Delta\theta^2 \rangle} \right) \times \sin(\pi k/N)^2 du. \quad \text{(B3)}$$

In this expression we average over the noise ξ and over the initial conditions $\langle |\theta_k(t_0)|^2 \rangle / N = g(k)$. In deriving Eq. (B3) we have assumed that $\langle \Delta\theta^2 \rangle$ is self-averaging, which implies that it is not correlated with ξ_k or $\theta_k(t_0)$ in the thermodynamic limit $N \to \infty$. In this limit we can replace $\frac{1}{N}\sum \to \int$ and $k/N \to k$. Considering $g(k) = \epsilon^2 c_\mu |\sin(\pi k)|^\mu$, Eq. (6) reads

$$\langle \Delta\theta^2 \rangle = \epsilon^2 4 c_\mu \int_0^1 \exp\left(2\dot\gamma \nu_k \int_{t_0}^{t} \frac{d\tau}{\langle \Delta\theta^2 \rangle} \right) \sin(\pi k)^{\mu+2} dk + \varsigma^2 4 \int_{t_0}^{t} \int_0^1 \exp\left(2\dot\gamma \nu_k \int_{u}^{t} \frac{d\tau}{\langle \Delta\theta^2 \rangle} \right) \times \sin(\pi k)^2 dk\, du. \quad \text{(B4)}$$

A bound for the contribution of the noise can be calculated by extending the lower limit of integration in the exponent from $u \to t_0$. This bound shows that the term induced by the noise can be neglected in the evolution for times $t - t_0 \ll c_\mu \epsilon^2/\varsigma^2$, which is equivalent to the condition that $\Delta\gamma/\dot\gamma \ll c_\mu \epsilon^2/\varsigma^2$. If the noise is considered to be introduced by thermal fluctuations, the required condition is that the system is strained fast enough toward the critical point to prevent thermalization.

A very different situation occurs under the reverse evolution from the critical point, i.e., the buckling process. We shall consider that the system is evolved until a time t_f smaller than the critical time and then the dynamics are reversed, which means changing $\dot\gamma \to -\dot\gamma$ in the evolution equation (B2). To simplify the backward evolution we will consider that there is no noise during the evolution; hence $\varsigma = 0$ and the only source of irreversibility comes from the accumulated noise in the forward evolution. The amplitude of the accumulated noise ε^2 must be much smaller that $\langle \Delta\theta^2 \rangle$ to ensure that the system is non-Brownian. Depending on the type of noise present in the evolution towards the critical point, the final deviation from the exact result might depend on the wave number. However, it can be shown that in most cases the particular choice of noise makes no difference for the backward evolution, so we consider for simplicity that the accumulated error is of the same order for every mode. Therefore, the initial condition is given by

$$\theta_k(t_f) = \theta_k(t_0) \exp\left(\dot\gamma \nu_k \int_{t_0}^{t_f} \frac{d\tau}{\langle \Delta\theta^2 \rangle} \right) + \varepsilon$$

and the reverse self-consistent equation is finally given by

$$\langle \Delta\theta^2 \rangle = 4 \int_0^1 g(k) \exp\left[2\dot\gamma \nu_k \left(\int_0^{t_f} \frac{d\tau}{\langle \Delta\theta^2 \rangle} - \int_{t_f}^{t} \frac{d\tau}{\langle \Delta\theta^2 \rangle} \right) \right] \sin(\pi k)^2 dk + \varepsilon^2 4 \int_0^1 \exp\left(-2\dot\gamma \nu_k \int_{t_f}^{t} \frac{d\tau}{\langle \Delta\theta^2 \rangle} \right) \sin(\pi k)^2 dk. \quad \text{(B5)}$$

Initially, the backward evolution is dominated by the reversible term, assuming that the noise amplitude $\varepsilon^2 \ll \langle \Delta\theta^2 \rangle$. Then the first term on the right-hand side of Eq. (B5) is proportional to $\epsilon^{-4/(1+\mu)} a_\mu (\gamma_c - \gamma)^{(3+\mu)/(1+\mu)}$, where $\gamma = \dot\gamma(2t_f - t)$ for $t > t_f$ and a_μ is a constant that only depends on μ (a_μ can be expressed in terms of Γ functions). We now estimate the time $t_{\rm noise}$ at which the noise term becomes of the same order of the reversible term:

$$\epsilon^{-4/(1+\mu)} a_\mu (\gamma_c - \gamma)^{(3+\mu)/(1+\mu)} \sim 4\varepsilon^2 \int_0^1 e^{-2\nu_k \rho(t)} \sin(\pi k)^2 dk, \quad \text{(B6)}$$

where $\rho(t) = \dot\gamma \int_{t_f}^{t} \frac{d\tau}{\langle \Delta\theta^2 \rangle}$. In this regime, while $t \ll t_{\rm noise}$ we can calculate $\rho(t)$ using the reversible evolution of $\langle \Delta\theta^2 \rangle$. In terms of the dimensionless strain γ one gets

$$\rho(t) \equiv \rho_{\rm r}(\gamma) = \frac{\epsilon^{4/(1+\mu)}(\mu+1)}{2 a_\mu (\gamma_c - \gamma_f)^{2/(1+\mu)}} \times \left[1 - \left(\frac{\gamma_c - \gamma}{\gamma_c - \gamma_f} \right)^{-2/(1+\mu)} \right], \quad \text{(B7)}$$

where $\gamma_f = \dot\gamma t_f$. The integral in Eq. (B9) can be expressed as

$$\int_0^1 e^{-2\nu_k \rho_{\rm r}(\gamma)} \sin(\pi k)^2 dk \equiv \frac{e^{4\rho_{\rm r}(\gamma)}}{2} [I_0(4\rho_{\rm r}(\gamma)) + I_1(4\rho_{\rm r}(\gamma))], \quad \text{(B8)}$$

where $I_0(x)$ and $I_1(x)$ are modified Bessel functions. Since we are considering exponentially small noise we need to reach values of $\rho(\gamma) \gg 1$. In this limit we can use the asymptotic expression for the Bessel function, which leads to the equation

$$\epsilon^{-4/(1+\mu)} a_\mu (\gamma_c - \gamma)^{(3+\mu)/(1+\mu)} \sim 4\varepsilon^2 e^{8\rho_{\rm r}(\gamma)} / \sqrt{8\pi \rho_{\rm r}(\gamma)}. \quad \text{(B9)}$$

The crossover strain $\gamma_{\rm noise}$ must take place when $\rho_{\rm r}(\gamma_{\rm noise}) \sim |\ln(\varepsilon)|/8$, which leads to the result $\gamma_c - \gamma_{\rm noise} \sim [\rho_{\rm r}(-\infty) - |\ln(\varepsilon)|/4]^{-(1+\mu)/2}$. The reversibility is then only lost if $\frac{|\ln(\varepsilon)|}{4\rho_{\rm r}(-\infty)} < 1$; however, due to the logarithmic dependence on the noise, this inequality is easily satisfied close to the critical point. If $\frac{|\ln(\varepsilon)|}{4\rho_{\rm r}(-\infty)} \ll 1$ one finds that the crossover time $t_{\rm noise} \sim t_f + \langle \Delta\theta(\gamma_f)^2 \rangle |\ln(\varepsilon)|/\dot\gamma$, above which the noise term becomes dominant and the reversible term can be neglected. Then the integral equation (B5) can be written as

$$\langle \Delta\theta^2 \rangle = \varepsilon^2 4 \int_0^1 \exp\left(-2\dot\gamma \nu_k \int_{t_f}^{t} \frac{d\tau}{\langle \Delta\theta^2 \rangle} \right) \sin(\pi k)^2 dk = \varepsilon^2 2 e^{4\rho(t)} [I_0(4\rho(t)) + I_1(4\rho(t))]. \quad \text{(B10)}$$

The integral form of $\rho(t)$ allow us to write

$$\rho(t) = \rho_r(\gamma_{\rm noise}) + \dot\gamma \int_{t_{\rm noise}}^{t} \frac{d\tau}{\langle \Delta\theta^2\rangle}.$$

Since $\rho_r(\gamma_{\rm noise}) \gg 1$ we can use the asymptotic behavior for the modified Bessel functions in Eq. (B10), which leads to

$$\langle \Delta\theta^2\rangle \approx 4\varepsilon^2 \frac{\exp\left(8\rho_r(\gamma_{\rm noise}) + 8\dot\gamma \int_{t_{\rm noise}}^{t} \frac{d\tau}{\langle \Delta\theta^2\rangle}\right)}{\sqrt{8\pi\rho_r(\gamma_{\rm noise})}}$$
$$= \langle \Delta\theta(t_{\rm noise})^2\rangle \exp\left(8\dot\gamma \int_{t_{\rm noise}}^{t} \frac{d\tau}{\langle \Delta\theta^2\rangle}\right). \quad \text{(B11)}$$

Finally, we obtain the asymptotic solution for the reverse evolution

$$\langle \Delta\theta^2\rangle \sim (\tilde\gamma_c - \gamma),$$

where the effective critical strain depends on the initial conditions $\tilde\gamma_c \approx \gamma_{\rm noise} + \langle \Delta\theta(t_{\rm noise})^2\rangle/8$, but the scaling exponent is universal.

APPENDIX C: SCALING OF $\omega_{\rm min}$ AND σ WITH STRAIN

We consider the ASM framework [12], in which overdamped hard spheres are driven under shear flow, and adopt the notation for dimensionless forces and velocities from the main text. The linear operator $\mathcal{S}$ and its transpose $\mathcal{S}^T$ are defined via the relations

$$\vec n_{ij}\cdot(\vec V_j - \vec V_i) \longleftrightarrow \mathcal{S}|V\rangle, \quad \text{(C1)}$$

$$\sum_{i(j)} \vec n_{ij}\tau_{ij} \longleftrightarrow \mathcal{S}^T|\tau\rangle, \quad \text{(C2)}$$

where $\vec n_{ij}$ are the unit vectors pointing from the center of particle i to the center of particle j and $i(j)$ are all the particles i that are in contact with particle j. We consider the limit of perfectly rigid particles, therefore the velocities $|V\rangle$ must preserve the distance between the centers of every pair of particles that are in contact, i.e., $\mathcal{S}|V\rangle = 0$. Decomposing the velocities to the driving affine flow and the nonaffine part $|V\rangle = |V^{\rm f}\rangle + |V^{\rm na}\rangle$, we require that drag forces $|F^{\rm drag}\rangle = |V^{\rm f}\rangle - |V\rangle$ balance the net forces on particles due to contacts

$$\mathcal{S}^T|\tau\rangle = -|F^{\rm drag}\rangle = |V\rangle - |V^{\rm f}\rangle. \quad \text{(C3)}$$

Operating on Eq. (C3) with $\mathcal{S}$ leads to Eq. (14). Inverting for the contact forces, we obtain

$$|\tau\rangle = -\mathcal{N}^{-1}\mathcal{S}|V^{\rm f}\rangle, \quad \text{(C4)}$$

where $\mathcal{N} \equiv \mathcal{S}\mathcal{S}^T$. Inserting Eq. (C4) into Eq. (C3) results in the nonaffine velocities

$$|V^{\rm na}\rangle = -\mathcal{S}^T\mathcal{N}^{-1}\mathcal{S}|V^{\rm f}\rangle. \quad \text{(C5)}$$

Denoting the kth particles' coordinates by $\vec R_k$ and the differences $\vec R_{ij} \equiv \vec R_j - \vec R_i$, the variation of the pairwise distance $r_\alpha \equiv \sqrt{\vec R_\alpha\cdot\vec R_\alpha}$ for the contact $\alpha = \langle ij\rangle$ under simple shear in the x-y plane is given by

$$\langle\alpha|\mathcal{S}|V^{\rm f}\rangle = \frac{\partial r_\alpha}{\partial\gamma} = \frac{\hat x\cdot\vec R_\alpha\vec R_\alpha\cdot\hat y}{r_\alpha}, \quad \text{(C6)}$$

where $\hat x$ and $\hat y$ denote Cartesian unit vectors. From here the stress is given by

$$\sigma = -\frac{\langle\tau|\mathcal{S}|V^{\rm f}\rangle}{\Omega} = \frac{\langle V^{\rm f}|\mathcal{S}^T\mathcal{N}^{-1}\mathcal{S}|V^{\rm f}\rangle}{\Omega} = \frac{\langle V^{\rm na}|V^{\rm na}\rangle}{\Omega}, \quad \text{(C7)}$$

where Ω is the dimensionless volume.

In our framework, the total derivatives of a regular observable $\mathcal{O}$ are taken as $\frac{d\mathcal{O}}{d\gamma} = \frac{\partial\mathcal{O}}{\partial\gamma} + \langle\frac{\partial\mathcal{O}}{\partial R}|V^{\rm na}\rangle$. As $\frac{\partial\mathcal{O}}{\partial\gamma}$ is always regular, whereas close to the critical point $|V^{\rm na}\rangle$ is singular [12], we approximate in the following $\frac{d\mathcal{O}}{d\gamma} \simeq \langle\frac{\partial\mathcal{O}}{\partial R}|V^{\rm na}\rangle$. We let $|W\rangle$ be a vector in the space of particles and calculate

$$\frac{d\mathcal{S}}{d\gamma}|W\rangle \simeq |(\langle V^{\rm na}|\mathcal{K}|W\rangle)|, \quad \text{(C8)}$$

where the contraction of $\mathcal{K}$ on a pair of any vectors $|U\rangle$,$|W\rangle$ is a vector in the space of contacts with components defined via

$$\vec U_{ij}\cdot\left(\frac{\overleftrightarrow{\mathcal{I}}}{r_{ij}} - \frac{\vec n_{ij}\vec n_{ij}}{r_{ij}}\right)\cdot\vec W_{ij} \longleftrightarrow \langle U|\mathcal{K}|W\rangle, \quad \text{(C9)}$$

where $\vec U_{ij} \equiv \vec U_j - \vec U_i$ and $\overleftrightarrow{\mathcal{I}}$ denotes the unit tensor. Notice that components of the vector $|(\langle W|\mathcal{K}|W\rangle)|$ are non-negative for any vector $|W\rangle$. Denoting by $|\phi_{\rm min}\rangle$ the normalized eigenvector of $\mathcal{N}$ associated with the minimal eigenvalue $\omega^2_{\rm min} = \langle\phi_{\rm min}|\mathcal{N}|\phi_{\rm min}\rangle$, the derivative of $\omega^2_{\rm min}$ with respect to strain is calculated as

$$\frac{d(\omega^2_{\rm min})}{d\gamma} \simeq 2|\langle\phi_{\rm min}|(\langle V^{\rm na}|\mathcal{K}\mathcal{S}^T|\phi_{\rm min}\rangle)|, \quad \text{(C10)}$$

since $\langle\phi_{\rm min}|\frac{d\phi_{\rm min}}{d\gamma}\rangle = 0$ from normalization. Close to the critical point the minimal mode has a finite coupling to the shear [16] (this simply comes from the fact that even for frictionless particles, at jamming the stress has a finite anisotropy, i.e., $\mu = \sigma/p > 0$), i.e., $\langle\phi_{\rm min}|\mathcal{S}|V^{\rm f}\rangle \sim ||\phi_{\rm min}|| \times ||\mathcal{S}|V^{\rm f}\rangle|| = ||\mathcal{S}|V^{\rm f}\rangle|| \sim \sqrt{N}$ (this last relation simply stem from the fact that the components of $\mathcal{S}|V^{\rm f}\rangle$ are of order one in our dimensionless units). Contact forces $|\tau\rangle$ [see Eq. (C4)] are thus dominated by the minimal mode, i.e.,

$$|\tau\rangle \sim -\frac{\langle\phi_{\rm min}|\mathcal{S}|V^{\rm f}\rangle|\phi_{\rm min}\rangle}{\omega^2_{\rm min}} \sim \frac{\sqrt{N}}{\omega^2_{\rm min}}|\phi_{\rm min}\rangle. \quad \text{(C11)}$$

Operating on this relation with $\mathcal{S}$ and using Eq. (C3), we find

$$\mathcal{S}^T|\phi_{\rm min}\rangle \sim \frac{\omega^2_{\rm min}}{\sqrt{N}}\mathcal{S}^T|\tau\rangle \sim \frac{\omega^2_{\rm min}}{\sqrt{N}}|V^{\rm na}\rangle. \quad \text{(C12)}$$

Inserting this expression for $\mathcal{S}^T|\phi_{\rm min}\rangle$ in Eq. (C10), we obtain

$$\frac{d(\omega^2_{\rm min})}{d\gamma} \sim \omega^2_{\rm min}\frac{|\langle\phi_{\rm min}|(\langle V^{\rm na}|\mathcal{K}|V^{\rm na}\rangle)|}{\sqrt{N}}. \quad \text{(C13)}$$

Since contact forces are positive for repulsive particles, close to the critical point where contact forces are dominated by the minimal mode, all components of $|\phi_{\rm min}\rangle$ are non-negative.

This is also true for the components of $|(\langle V^{\rm na}|\mathcal{K}|V^{\rm na}\rangle)\rangle$ by construction. Thus we expect for the overlap

$$\langle\phi_{\rm min}|(\langle V^{\rm na}|\mathcal{K}|V^{\rm na}\rangle)\rangle \sim ||\phi_{\rm min}|| \times ||\langle V^{\rm na}|\mathcal{K}|V^{\rm na}\rangle|| = ||\langle V^{\rm na}|\mathcal{K}|V^{\rm na}\rangle||.$$

We finally assume that the *relative* nonaffine displacement, of order $(||\langle V^{\rm na}|\mathcal{K}|V^{\rm na}\rangle||/\sqrt{N})^{1/2}$, is the order of the relative nonaffine velocities between particles, by definition of order $||V^{\rm na}||/\sqrt{N}$. This assumption is consistent with our results on the buckling of the one-dimensional chain, where it applies. This assumption implies that

$$\frac{\langle\phi_{\rm min}|(\langle V^{\rm na}|\mathcal{K}|V^{\rm na}\rangle)\rangle}{\sqrt{N}} \sim \frac{||V^{\rm na}||^2}{N}. \tag{C14}$$

Returning to Eq. (C7), we use Eq. (C11) for the forces to obtain

$$\sigma \sim \frac{||V^{\rm na}||^2}{\Omega} \sim \frac{\langle\phi_{\rm min}|\mathcal{S}|V^{\rm f}\rangle^2}{\Omega\omega_{\rm min}^2} \sim \frac{N}{\Omega\omega_{\rm min}^2} \sim \frac{1}{\omega_{\rm min}^2}. \tag{C15}$$

Finally, using Eqs. (C14) and (C15) in Eq. (C13), we find that $\frac{d(\omega_{\rm min}^2)}{d\gamma} \sim O(1)$ or $\omega_{\rm min} \sim \sqrt{\gamma-\gamma_c}$ with $\gamma_c < \gamma$. A straightforward consequence of the scalings $\omega_{\rm min} \sim \sqrt{\gamma-\gamma_c}$ and $\sigma \sim 1/\omega_{\rm min}^2$ [see Eq. (C15)] is a prediction for the relaxation of the stress $\sigma \sim 1/(\gamma-\gamma_c)$ or, alternatively,

$$\frac{d\sigma}{d\gamma} \sim -\sigma^2\,, \tag{C16}$$

which is validated numerically in Fig. 7(b).

APPENDIX D: NUMERICAL METHODS

Data for the flow of hard particles within the ASM framework [12] are generated using the algorithm described in [26]. We have simulated a binary mixture of large and small disks in two dimensions with $N = 4096$ particles, setting the ratio of radii of large and small particles to 1.4. Systems were deformed under simple shear with Lees-Edwards periodic boundary conditions for strains of at least 300% before statistics were collected. We simulated systems at various packing fractions ranging from $\phi = 0.820$ to 0.840.

The same algorithm described in [26] is straightforwardly adapted for deforming networks of rigid rods by keeping the topology of the networks fixed. Initial floppy networks of rods with coordination $z < 2d$ were created as described in [20]. We have simulated networks of $N = 4096$ and $N = 40\,000$ nodes and coordinations varying between $z = 3.6$ and 3.95. Networks were deformed under simple shear with Lees-Edwards periodic boundary conditions until the dimensionless stress reached $\sigma \approx 10^6$. Then the shear was reversed [see, for example, the stress-strain signal of Fig. 3(a)] and data were collected. Responses to point perturbations and velocity correlations were measured in the larger networks, whereas the spectral analysis as displayed in Fig. 4 was performed on the smaller networks. The response to a point perturbation [Figs. 2(c), (5), 7(c), and 7(d)] at a bond α is calculated by solving the equation $\mathcal{N}|f\rangle = |\alpha\rangle$ for $|f\rangle$ and then calculating $|V\rangle = \mathcal{S}^T|f\rangle$ (see Appendix C for definitions of $\mathcal{S}$ and $\mathcal{N}$). The derivatives $d\sigma/d\gamma$ were calculated by finite differences. Linear chains with $N = 10\,000$ nodes were deformed under extensional flow with periodic boundary conditions using the same method used for random floppy networks.

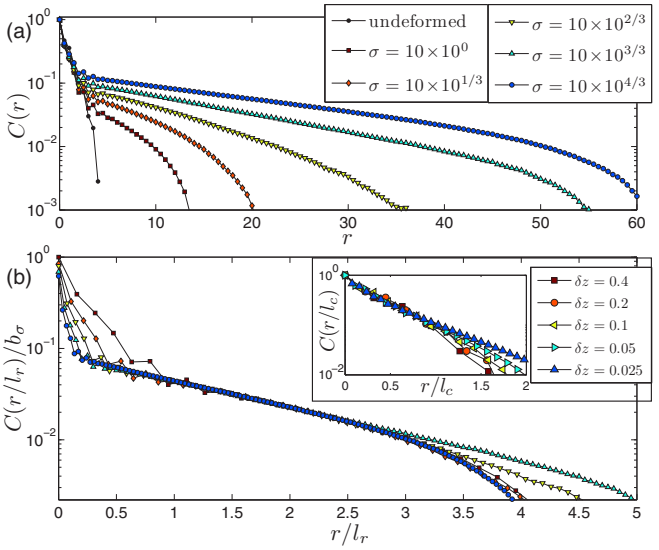

FIG. 8. (Color online) Velocity correlations $C(r)$ for networks under shear. (a) The raw correlation functions have an initial exponential decay on the length scale $l_c \sim 1/\sqrt{\delta z}$. We also show the velocity correlations measured in an undeformed isotropic network of the same coordination (black dots), demonstrating that the initial decay occurs on the same length scale, independent of the stress. (b) The correlation functions rescaled by constants b_σ, which are chosen such that the functions collapse with the second length scale l_r, scaling as $l_r \sim \sqrt{\sigma}$ at fixed z. We find numerically $b_\sigma \sim \ln(\sigma)$. In the inset of (b) we plot the velocity correlations measured in undeformed isotropic networks with various coordinations.

APPENDIX E: VELOCITY CORRELATIONS IN STRAINED RANDOM NETWORKS

In Fig. 8 the velocity correlations $C(r) \equiv \frac{\langle\vec{V}_i\cdot\vec{V}_j\rangle}{\langle V^2\rangle}$ vs distance r between particles i and j are plotted for networks of $N = 40\,000$ nodes with $\delta z = 0.2$ in two dimensions, at various stresses. We find that $C(r)$ initially decays exponentially on the scale $l_c \sim 1/\sqrt{\delta z}$ and then crosses over to an exponential decay on the length scale $l_r \sim \sqrt{\sigma}$. These correlation functions are similar to the velocity response to a point perturbation presented in Fig. 5. Notice in particular the two exponential decays on the length scale l_c at short distance and l_r in the far field.

[1] GDR MiDi, Eur. Phys. J. E **14**, 341 (2004).
[2] O. Pouliquen, Phys. Rev. Lett. **93**, 248001 (2004).
[3] F. da Cruz, S. Emam, M. Prochnow, J.-N. Roux, and F. Chevoir, Phys. Rev. E **72**, 021309 (2005).
[4] F. Boyer, E. Guazzelli, and O. Pouliquen, Phys. Rev. Lett. **107**, 188301 (2011).
[5] R. Lespiat, S. Cohen-Addad, and R. Höhler, Phys. Rev. Lett. **106**, 148302 (2011).

[6] F. Blanc, F. Peters, and E. Lemaire, J. Rheol. **55**, 835 (2011).
[7] A. Tordesillas and M. Muthuswamy, J. Mech. Phys. Solids **57**, 706 (2009).
[8] C. Heussinger and J.-L. Barrat, Phys. Rev. Lett. **102**, 218303 (2009).
[9] D. J. Durian, Phys. Rev. Lett. **75**, 4780 (1995).
[10] P. Olsson and S. Teitel, Phys. Rev. Lett. **99**, 178001 (2007).
[11] T. Hatano, Phys. Rev. E **79**, 050301(R) (2009).
[12] E. Lerner, G. Düring, and M. Wyart, Proc. Natl. Acad. Sci. USA **109**, 4798 (2012).
[13] B. Andreotti, J.-L. Barrat, and C. Heussinger, Phys. Rev. Lett. **109**, 105901 (2012).
[14] P. Olsson, Phys. Rev. E **81**, 040301 (2010).
[15] G. Düring, E. Lerner, and M. Wyart, Soft Matter **9**, 146 (2013).
[16] E. Lerner, G. Düring, and M. Wyart, Europhys. Lett. **99**, 58003 (2012).
[17] J. Maxwell, Philos. Mag. **27**, 294 (1864).
[18] C. Calladine, Int. J. Solids Struct. **14**, 161 (1978).
[19] P. R. Onck, T. Koeman, T. van Dillen, and E. van der Giessen, Phys. Rev. Lett. **95**, 178102 (2005).
[20] M. Wyart, H. Liang, A. Kabla, and L. Mahadevan, Phys. Rev. Lett. **101**, 215501 (2008).
[21] M. Sheinman, C. P. Broedersz, and F. C. MacKintosh, Phys. Rev. E **85**, 021801 (2012).
[22] C. Heussinger, B. Schaefer, and E. Frey, Phys. Rev. E **76**, 031906 (2007).
[23] O. Lieleg, M. M. A. E. Claessens, C. Heussinger, E. Frey, and A. R. Bausch, Phys. Rev. Lett. **99**, 088102 (2007).
[24] S. B. Lindstrom, A. Kulachenko, L. Jawerth, and D. A. Vader, Soft Matter **9**, 7302 (2013).
[25] K. Sun, A. Souslov, X. Mao, and T. C. Lubensky, Proc. Natl. Acad. Sci. USA **109**, 12369 (2012).
[26] E. Lerner, G. Düring, and M. Wyart, Comput. Phys. Commun. **184**, 628 (2013).
[27] C. Storm, J. Pastore, F. MacKintosh, T. Lubensky, and P. Janmey, Nature (London) **435**, 191 (2005).
[28] B. P. Tighe, E. Woldhuis, J. J. C. Remmers, W. van Saarloos, and M. van Hecke, Phys. Rev. Lett. **105**, 088303 (2010).
[29] D. L. Henann and K. Kamrin, Proc. Natl. Acad. Sci. USA **110**, 6730 (2013).
[30] M. Bouzid, M. Trulsson, P. Claudin, E. Clément, and B. Andreotti, Phys. Rev. Lett. **111**, 238301 (2013).